European Journal of Medicinal Chemistry xxx (xxxx) xxx

Contents lists available at ScienceDirect

European Journal of Medicinal Chemistry

journal homepage: http://www.elsevier.com/locate/ejmech

Research paper

Novel thiazolidinedione-hydroxamates as inhibitors of *Mycobacterium tuberculosis* virulence factor Zmp1

Veronika Šlachtová [a], Marek Šebela [b], Eveline Torfs [c], Lauren Oorts [c], Davie Cappoen [c], Karel Berka [d], Václav Bazgier [d], Lucie Brulíková [a, *]

[a] Department of Organic Chemistry, Faculty of Science, Palacký University, 17. listopadu 12, 771 46, Olomouc, Czech Republic
[b] Department of Protein Biochemistry and Proteomics, Centre of the Region Haná for Biotechnological and Agricultural Research, Faculty of Science, Palacký University, Šlechtitelů 27, 783 71, Olomouc, Czech Republic
[c] Laboratory of Microbiology, Parasitology and Hygiene (LMPH), S7, Faculty of Pharmaceutical, Biomedical and Veterinary Sciences, University of Antwerp, Wilrijk, Belgium
[d] Department of Physical Chemistry, Regional Centre of Advanced Technologies and Materials, Faculty of Science, Palacky University, 17. listopadu 12, 771 46, Olomouc, Czech Republic

ARTICLE INFO

Article history:
Received 2 May 2019
Received in revised form
7 August 2019
Accepted 23 October 2019
Available online xxx

Keywords:
Zmp1
Mycobacterium tuberculosis
Thiazolidinediones
Hydroxamates
MALDI-TOF

ABSTRACT

Zinc metalloprotease 1 (Zmp1) is an extracellular enzyme, which has been found essential for the intracellular survival and pathogenesis of *Mycobacterium tuberculosis*. In this work, we designed and synthesized a series of novel thiazolidinedione-hydroxamates and evaluated *in silico* their drug-likeness behavior. Then, their inhibitory properties towards a recombinant Zmp1 from *Mycobacterium tuberculosis* were analyzed by MALDI-TOF MS. Nine of the tested compounds were found to inhibit the enzymatic reaction more effectively than the generic metalloprotease inhibitor phosphoramidon. Furthermore, the synthesized thiazolidinedione-hydroxamate hybrids were evaluated for their *in vitro* antimycobacterial activity and acute cytotoxicity using whole-cell assays. Results showed that none of the hybrids exhibited acute cytotoxicity against RAW264.7 macrophages. Whereas extracellular antimycobacterial activity was limited, RAW264.7 macrophage infection results showed that a majority of the hybrids inhibited the intracellular growth of *Mycobacterium tuberculosis* at a concentration of 100 and 10 μM. The thiazolidinedione-hydroxamate compound **2n** was considered to be the best candidate of the evaluated library.

1. Introduction

Tuberculosis (TB), an infectious disease predominantly caused by the bacillus *Mycobacterium tuberculosis (Mtb)* still poses a major and enduring global health threat [1]. The infectious disease remains one of the top 10 causes of death and is, additionally, the leading cause of death due to a single infectious agent. In 2017, approximately 10 million people developed active TB disease and over 1.6 million persons died as a result [2]. Furthermore, the epidemic is fueled by the current HIV/AIDS pandemic and ever-increasing emergence of anti-TB drug resistance [2]. Moreover, there is only a limited number of drugs available on the market for the treatment of multidrug-resistant (MDR) and extensively drug-resistant (XDR) TB. Additionally, treatment is less efficient and associated with serious side effects [3]. Without doubt, the discovery of entirely new compounds with an alternative mechanism of action to the existing therapeutics and directed towards unknown targets of *Mtb* becomes more and more desirable [4,5].

One attractive mycobacterial target is represented by the promising and validated 20S proteasome protein, which is necessary for persistence in mice and vitality of the bacterium in pathogenesis as it protects *Mtb* against nitrosative stress from the host [6]. More recently, another interesting mycobacterial enzyme with protease activity was identified, i.e. zinc metalloprotease 1 (Zmp1). The enzyme is found to be essential for the intracellular survival and pathogenesis of *Mtb* [7–11]. In 2008, Master et al. illustrated that Zmp1 affects the macrophage phagosome maturation via suppression of inflammasome activation and subsequent phagolysosome formation, desired for the full clearance of the invalid pathogens (Fig. 1). The exact action mechanism of Zmp1 in the

* Corresponding author.
E-mail address: lucie.brulikova@upol.cz (L. Brulíková).

https://doi.org/10.1016/j.ejmech.2019.111812
0223-5234/

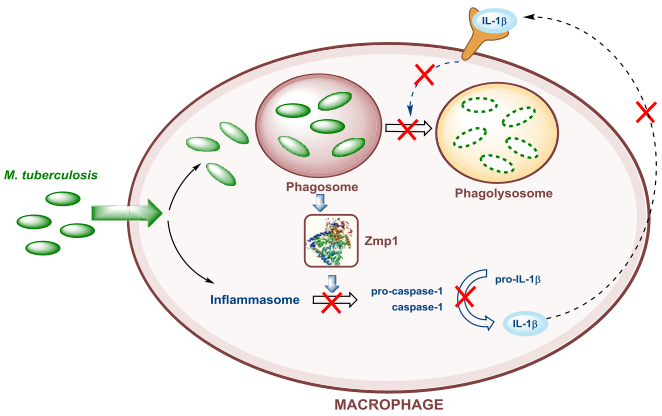

Fig. 1. Inhibition of the phagosome maturation process by mycobacterial Zmp1 (this figure was adopted from Ferraris and Rizzi) [11].

pathogenesis, however, has not been fully elucidated. Though, there is evidence that the zinc metalloprotease, a type of enzyme which can carry out diverse functions in pathogenic microorganisms, may be released from *Mtb* and act on the activation of the caspase-1/interleukin-1β inflammasome, ultimately disrupting phagolysosome formation and *Mtb* clearance [8]. Therefore, Zmp1 and its inhibition leading to virulence attenuation may also represent a potentially useful drug target and are worthy of further investigation.

The molecular structures of the mycobacterial 20S proteasome and Zmp1 are markedly different. Unlike the monomeric Zmp1 [7], 20S proteasome is a large barrel-shaped oligomer: 7 α-subunits are arranged into an α-ring and 7 β-subunits form a β-ring. These rings are stacked to a symmetric complex of $\alpha_{1\text{-}7}\beta_{1\text{-}7}\beta_{1\text{-}7}\alpha_{1\text{-}7}$ [12]. The active site of Zmp1 appears between the two structural domains rich in α-helices and contains a catalytic zinc ion in tetrahedral coordination. Because of the presence of hydrophobic residues, peptide substrates with a large hydrophobic P1' side chain (e.g. Phe, Leu, Ile) are well accommodated. There is also a secondary binding pocket available at the active site, with arginine residues, which has been suggested a promising docking site for inhibitors [7]. Conversely, the proteolytic mechanism of 20S proteasome involves the N-terminal threonine residue of each β-subunit [13]. The arrangement of the substrate binding pocket in *M. tuberculosis* 20S proteasome allows versatility in degrading of hydrophobic, basic as well as acidic peptide substrates [12]. The enzyme shows not only a different mechanism but also substrate and cleavage specificity compared to Zmp1. Thus, it is clear that the designing of new inhibitors of these two enzyme targets has to follow unique principles and approaches.

To date, only a few examples of Zmp1 inhibitors are known [14–18]. In 2014, the first selective *Mtb* Zmp1 inhibitors emerged, when the Botta group identified active structures by combining an *in silico* structure-based inhibitor design and biochemical studies (Fig. 2) [14]. Most of the defined structures in their study comprised the rhodanine skeleton that further served as a basic structural motif for the development of other Zmp1 inhibitors [15–18]. The most potent Zmp1 inhibitor to date was identified in the latest study from 2018 [16] when Paolino et al. described a series of 8-hydroxyquinolines modified with a hydroxamate substitution as the zinc-binding group.

In the present study, a protocol for synthetic preparation of thiazolidinedione-hydroxamates was developed. All synthesized compounds were evaluated for their antimycobacterial activity. In addition, the inhibitory properties of the studied compounds towards a recombinant Zmp1 from *Mycobacterium tuberculosis* were analyzed by MALDI-TOF MS.

2. Results and discussion

Based on the biological significance of both thiazolidinedione scaffold [19–21] and known hydroxamate-based zinc-binding group (ZBG) [22,23], a new library of thiazolidinedione-hydroxamate hybrids was designed and synthesized (Fig. 3). Two lipophilic hydroxamates as privileged scaffolds in a multitude of medicinally useful agents were selected for our initial studies [23–25]. Thiazolidinedione heterocycle may further be modified by various benzylidenes or alkylidenes according to various known biologically active structures [19]. Furthermore, the thiazolidinedione and hydroxamate scaffolds are connected via an appropriate linker R^2, where two simple variants were selected for the initial study.

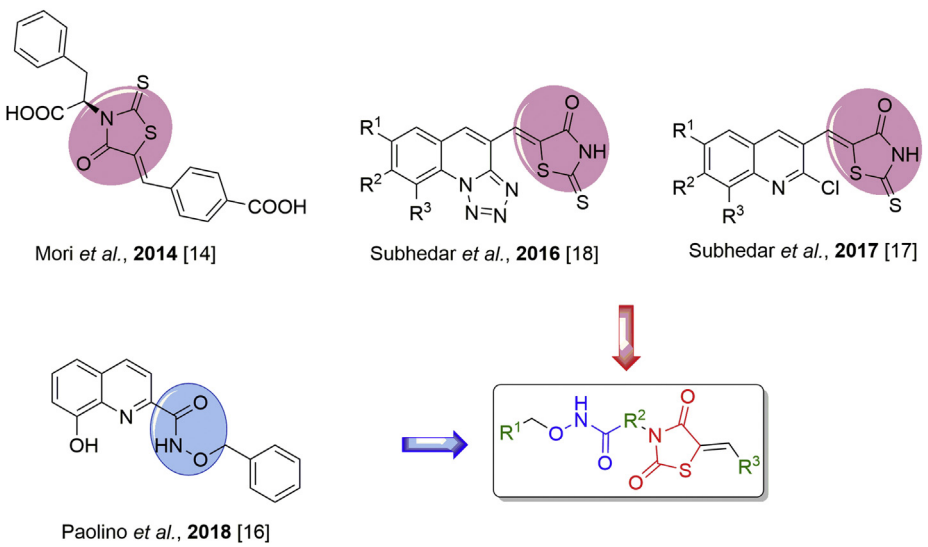

Fig. 2. Examples of known Zmp1 inhibitors and design of novel compounds.

Please cite this article as: V. Šlachtová et al., Novel thiazolidinedione-hydroxamates as inhibitors of *Mycobacterium tuberculosis* virulence factor Zmp1, European Journal of Medicinal Chemistry, https://doi.org/10.1016/j.ejmech.2019.111812

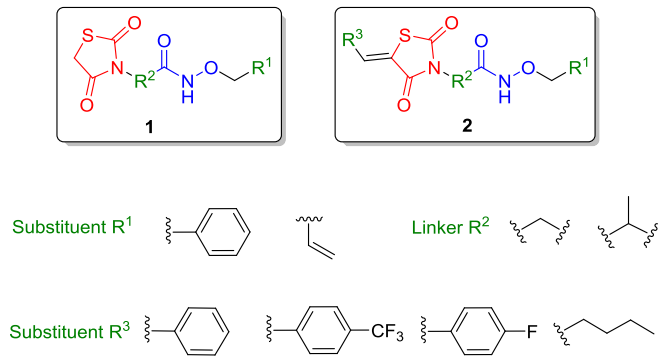

Fig. 3. Structures selected for the study.

3. Chemistry

First, simple thiazolidinedione-unsubstituted hydroxamates **1** were generated (Scheme 1). The initial thiazolidinedione **3** was synthesized according to a previously described procedure [26] and reacted with methyl bromoacetate or methyl 2-bromopropionate giving compounds **4**. This step was followed by the acid-catalyzed hydrolysis resulting in carboxylic acids **5.** The desired compounds **1** were obtained after a coupling reaction of the carboxylic acids **5** with either *O*-allylhydroxylamine hydrochloride or *O*-benzylhydroxylamine hydrochloride using *N*-(3-dimethylaminopropyl)-*N*′-ethyl carbodiimide hydrochloride (EDC.HCl) under aqueous conditions in moderate yields (see Table 1).

Next, hydroxamates **2** were synthesized (Scheme 1). The synthetic procedure was initiated with Knoevenagel condensation of thiazolidinedione **4** with various aldehydes to reach compounds **6**. Then a substitution with methyl bromoacetate or methyl 2-bromopropionate gave compounds **7**. After the acid-mediated hydrolysis of **7,** the resulting carboxylic acids **8** were coupled with either *O*-allylhydroxylamine hydrochloride or *O*-benzylhydroxylamine hydrochloride using EDC.HCl to give hydroxamates **2** in yields ranging from 31 to 75% (see Table 2). The lower yields were caused by losses during column chromatography.

Finally, we assessed the stereochemical outcome of our synthetic protocol. The formation of two geometrical isomers *E* or *Z* after Knoevenagel condensation is possible. These two isomers can easily be distinguished by their ^{1}H NMR spectral characteristics. It is well known that the benzylidine proton appears above 7.90 ppm for *Z* isomer and below 7.42 ppm for *E* isomer [27,28]. The measured NMR data confirmed the formation of *Z* isomers for all our products. Moreover, the final compounds containing a stereogenic centre were analyzed by supercritical fluid chromatography (SFC). All analyses confirmed the racemic form of both mentioned derivatives (See Supplementary).

3.1. In silico prediction of drug-likeness properties

To select those compounds suitable for further screening, *in silico* physicochemical and pharmacokinetic parameters of the thiazolidinedione-hydroxamates were predicted using the knowledge-based FAF*Drugs*4 [29] and admetSAR [30] software tools [6,31]. Narrowing the library to a series of compounds with a favourable drug-likeness and no toxicity alerts avoids futile investment in compounds with possible undesirable effects in later stages of the drug discovery and development cascade. For each hybrid, the predicted drug-likeness parameters are shown in Table 3, whereas ranges of such parameters followed by 95% of known drugs are also added in the footnotes [32,33]. The results revealed that the synthesized thiazolidinedione-hydroxamates meet the Lipinski's rule of five as the predicted values of the molecular weight, *n*-octanol, and water partition coefficient, hydrogen bond acceptors and hydrogen-bond donors parameters fall within the prescribed ranges. Furthermore, the number of atoms was also found within the range, improving drug-likeness [29]. Aqueous solubility was forecasted to be good for all thiazolidinedione-hydroxamates, except for **2g**, for which it was predicted to be reduced with a $\log S^W$ of −5.22. The thiazolidinedione-hydroxamates were also considered to have a good oral bioavailability, based on Verber's rule [34]. All hybrids were designated to class III considering acute oral toxicity, which reveals that the compounds should possess fairly high lethal doses (i.e. $LD_{50} = 0.5-5$ g/kg) and can be considered druggable. As for mutagenicity (Ames test), there were no alerts indicated. In contrast, another rule of thumb such as the GSK 4/400 rule, which anticipates higher risks of toxicity, interactions with off-targets or difficulties during development if the logP and the molecular weight is larger than 4 and 400, respectively, suggested that **2e** and **2g** could be less druggable [29]. Though, the overall results indicate that the synthesized thiazolidinedione-hydroxamates generally do possess drug-likeness behavior. Therefore, all derivatives are selected for further investigation, except the compounds **2e** and **2g**.

3.2. Inhibitory activity towards Zmp1

The inhibitory properties of the studied compounds towards a recombinant zinc metallopeptidase (Zmp1) from *Mtb* were

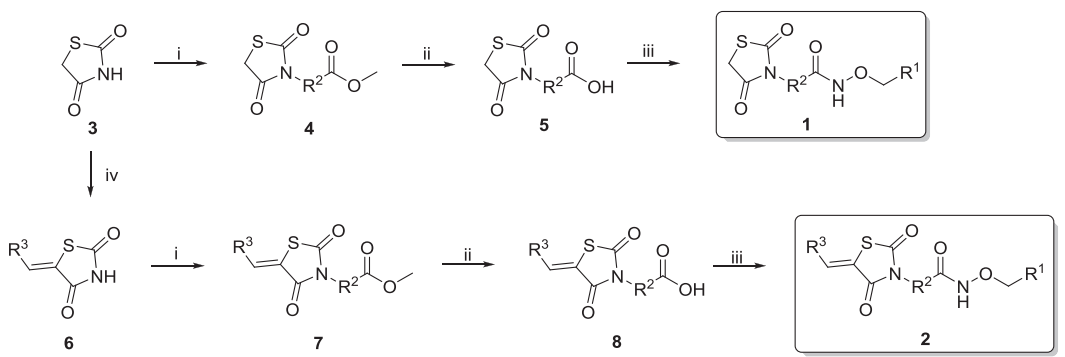

Scheme 1. Synthesis of model compounds **1** and **2**.
Reagents and conditions: (i) methyl bromoacetate or methyl 2-bromopropionate, NaH, DMF dry, rt, on; (ii) HBr (40%), reflux, 5 h; (iii) *O*-allylhydroxylamine hydrochloride or *O*-benzylhydroxylamine hydrochloride, EDC.HCl, H_2O, rt, 2 h; (iv) aldehyde, piperidine, EtOH, reflux, 5 h.

Please cite this article as: V. Šlachtová et al., Novel thiazolidinedione-hydroxamates as inhibitors of *Mycobacterium tuberculosis* virulence factor Zmp1, European Journal of Medicinal Chemistry, https://doi.org/10.1016/j.ejmech.2019.111812

Table 1
Overview of synthesized products **1**.

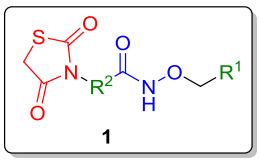

Entry	R^1	R^2	Yield[a] [%]
1a			49
1b			55
1c			61
1d			52

[a] Isolated yield after purification.

Table 2
Overview of synthesized products **2**.

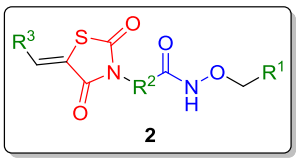

Entry	R^1	R^2	R^3	Yield[a] [%]
2a				58
2b				51
2c				64
2d				62
2e			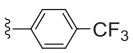	49
2f			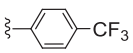	50
2g			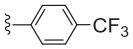	48
2h			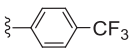	31
2i			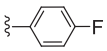	35
2j			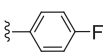	40
2k				60
2l				56
2m				75
2n				75
2o				45
2p				45

[a] Isolated yield after purification.

analyzed by matrix-assisted laser desorption/ionization-time of flight mass spectrometry (MALDI-TOF MS). The reaction mixture contained human angiotensin II as a substrate and the respective inhibitor. The proteolytic digestion of angiotensin II (*m/z* 1046) produced two peptide fragments providing characteristic signals in the mass spectrum, namely DRVY (*m/z* 552) and IHPF (*m/z* 513), in accordance with the literature [35] and as confirmed by tandem MS (MS/MS) analyses (not shown). The production of the fragments was accompanied by a simultaneous decrease in the angiotensin II signal (Supplementary Figs. S1–2).

MALDI is generally not considered a robust ionization technique for quantitative measurements, but a growing number of reports have documented its applicability for quantifying peptides [36]. This stems from reduced experimental difficulties because of the ongoing technological improvement of the instruments [37]. In this work, we eliminated both sample-to-sample and shot-to-shot variability of peak intensities by reading intensity ratios of the reaction product at *m/z* 552 and substrate at *m/z* 1046 in mass spectra averaged from 1000 laser shots. Finally, the inhibition rate was calculated from the ratio of the determined time-dependence slopes for inhibited and control reaction (Supplementary Table S1). Fig. 4 shows the obtained results. All compounds were found to inhibit the enzymatic reaction but the existing structural differences were reflected in their inhibitory strength. The most potent inhibitors were **2c**, **2k-m**, and **1b** (which inhibited almost completely), whereas **2d** and **2g** inhibited only by less than 20%.

Using the measured inhibition percentages, IC_{50} (half-maximal inhibitory concentration) values of the inhibitors can be estimated (100% activity for [I] = 0 μM) and they appear in the range of 20–160 μM. Experimental IC_{50} values were obtained with three different inhibitor concentrations for **2n** (18 μM) and **2e** (38 μM), which represent highly efficient and medium-efficient inhibitors from the studied group, respectively. These numbers correspond to inhibition constants described for some other Zmp1 inhibitors [6,14,38].

Supplementary table (Table S2) shows a graphic interpretation of the influence of chemical functional groups on the inhibitory properties. The analyzed hybrid compounds can be divided into five clusters according to the substituent at the thiazolidinedione moiety (R^3): without any substitution, with a benzylidene, fluorobenzylidene, trifluorobenzylidene, and pentylidene substituting group. In each cluster, the presence of either a benzyl or allyl substitution at the hydroxamate moiety (R^1) was considered, plus a possible methyl group in the linker (R^2). As can be seen, the benzyl group at the hydroxamate function resulted predominantly in a lower inhibition potency compared to the allyl group at this position for the hybrid compounds with both non-substituted and trifluorbenzylidene-substituted thiazolidinedione ring. An opposite trend was found for those containing the benzylidene-substituted thiazolidinedione ring, whereas no clear trend was observed for the other two clusters. The methyl group presence in

Please cite this article as: V. Šlachtová et al., Novel thiazolidinedione-hydroxamates as inhibitors of *Mycobacterium tuberculosis* virulence factor Zmp1, European Journal of Medicinal Chemistry, https://doi.org/10.1016/j.ejmech.2019.111812

Table 3
In silico predicted physicochemical and pharmacokinetic parameters of the thiazolidinedione-hydroxamates.

Compound	MW[a]	LogP[b]	HBD[c]	HBA[d]	No. of atoms[e]	Rotatable bonds[f]	logSw[g]	Solubility Forecast Index	Oral bioavailability (Veber's rule]	4/400	Ames test toxicity	Acute oral toxicity
1a	280.3	1.14	1	6	19	5	−2.11	Good	Good	Good	Non	III
1b	230.24	0.29	1	6	15	5	−1.12	Good	Good	Good	Non	III
1c	294.33	1.54	1	6	20	5	−2.44	Good	Good	Good	Non	III
1d	244.27	0.69	1	6	16	5	−1.46	Good	Good	Good	Non	III
2a	368.41	3.26	1	6	26	6	−3.99	Good	Good	Good	Non	III
2b	318.35	2.41	1	6	22	6	−3.06	Good	Good	Good	Non	III
2c	382.43	3.67	1	6	27	6	−4.32	Good	Good	Good	Non	III
2d	332.37	2.82	1	6	23	6	−3.4	Good	Good	Good	Non	III
2e	436.41	4.15	1	6	30	7	−4.9	Good	Good	Bad	Non	III
2f	386.35	3.30	1	6	26	7	−3.97	Good	Good	Good	Non	III
2g	450.43	4.55	1	6	31	7	−5.22	Reduced	Good	Bad	Non	III
2h	400.37	3.70	1	6	27	7	−4.3	Good	Good	Good	Non	III
2i	386.4	3.36	1	6	27	6	−4.17	Good	Good	Good	Non	III
2j	336.34	2.51	1	6	23	6	−3.23	Good	Good	Good	Non	III
2k	400.42	3.77	1	6	28	6	−4.5	Good	Good	Good	Non	III
2l	350.36	2.92	1	6	24	6	−3.57	Good	Good	Good	Non	III
2m	348.42	3.52	1	6	24	8	−3.79	Good	Good	Good	Non	III
2n	298.36	2.67	1	6	20	8	−2.84	Good	Good	Good	Non	III
2o	362.44	3.92	1	6	25	8	−4.12	Good	Good	Good	Non	III
2p	312.38	3.07	1	6	21	8	−3.18	Good	Good	Good	Non	III

[a] Molecular Weight (MW; 130 to 725).
[b] Log partition coefficient between *n*-octanol and water (−2 to 6.5).
[c] Number of hydrogen bond donors (0–6).
[d] Number of hydrogen acceptors (2–20).
[e] Number of atoms (20–70).
[f] Number of rotatable bonds (0–15).
[g] Log aqueous solubility (−6.5 to 0.5).

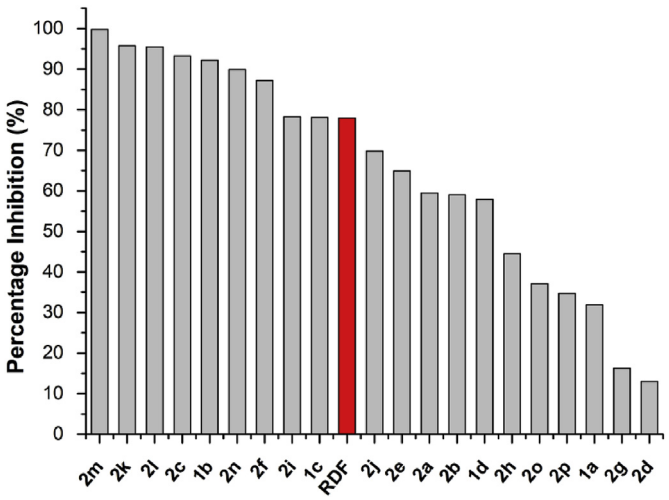

Fig. 4. Inhibitory activity toward Zmp1. Inhibition rate at a given inhibitor concentration of 40 μM was calculated by inverting the ratio of slopes for inhibited and control reaction. Phosphoramidon (RDF) was used as a reference at a final concentration of 40 μM [16].

the linker resulted in lower inhibitory properties when compared to the counterparts without this group, for the compounds with pentylidene and trifluorbenzylidene substitutions at the thiazolidinedione ring. It was the opposite for those with the fluorobenzylidene substitution. Generally, this interpretation indicates that the measured inhibition data reflect a structure-based interaction with the enzyme molecule as they are not fully random.

3.3. *In vitro* biological activity

Following the synthesis and enzymatic assays, the thiazolidinedione-hydroxamate hybrids were evaluated for their *in vitro* activity against *Mycobacterium tuberculosis* H37Ra using a whole-cell assay. Antimycobacterial potency was assessed using resazurin, as previously reported [39]. The results were expressed as the IC_{50}, and also minimal inhibitory concentration (MIC) at which the mycobacterial growth is reduced by 90% (Table 4). In parallel, the acute cytotoxicity of the thiazolidinedione-hydroxamates against the eukaryotic RAW264.7 macrophage cell line was studied using a previously reported neutral red uptake (NRU) assay [40]. The cytotoxic concentration (CC_{50}) of a compound is defined as the concentration at which the NRU by the cells is reduced by 50% (Table 4). The selectivity index (SI) of the synthesized compounds was calculated by dividing the CC_{50} with the MIC (Table 4). Results showed that most of the thiazolidinedione-hydroxamates showed no significant antimycobacterial activity against extracellular *Mtb* H37Ra, i.e. IC_{50} and MIC values > 64 μM (Table 4). The hybrids **2f**, **2k**, **2l**, **2m** and **2n** showed a low antimycobacterial potency with IC_{50} values of 51.7, 44.4, 60.0, 55.0 and 42.2 respectively. For **2n**, a MIC value of 61.8 could be calculated. Except for **2o**, none of the compounds exhibited acute cytotoxicity against RAW264.7 macrophages, i.e. CC_{50} values > 128 μM (Table 4). Only **2o** showed a low cytotoxic effect with a CC_{50} value of 43.9 μM. Though, this effect did not exceed the cytotoxic effect of the reference drug tamoxifen ($CC_{50} = 11.1$ μM). As a result, a SI of at least 2.1 and 0.7, respectively, could be calculated for **2n** and **2o**. Although only a low antimycobacterial activity against extracellular *Mtb* H37Ra was present, **2n** showed to be the most potent of the evaluated hybrids. Interestingly, this compound belonged to those providing the strongest inhibitory properties towards the mycobacterial enzyme Zmp1.

As the thiazolidinedione-hydroxamate hybrids were designed as Zmp1-inhibitors, the *in vitro* antimycobacterial activity of the compounds against intracellular residing *Mtb* H37Ra bacilli was assessed as well. The intracellular activity was studied using a luminometric macrophage infection assay [41]. Based on the luminescent signal of the synthesized compounds and untreated control, the obtained results were expressed as inhibition

Table 4
In vitro antimycobacterial activity and acute cytotoxicity results.

Compound	IC_{50} (μM)[a]	MIC (μM)[b]	CC_{50} (μM)[c]	SI[d]
1a	>64	>64	>128	ND
1b	>64	>64	>128	ND
1c	>64	>64	>128	ND
1d	>64	>64	>128	ND
2a	>64	>64	>128	ND
2b	>64	>64	>128	ND
2c	>64	>64	>128	ND
2d	>64	>64	>128	ND
2e	59.5	>64	>128	ND
2f	51.7	>64	>128	ND
2g	>64	>64	>128	ND
2h	>64	>64	>128	ND
2i	>64	>64	>128	ND
2j	>64	>64	>128	ND
2k	>64	>64	>128	ND
2l	60.0	>64	>128	ND
2m	55.0	>64	>128	ND
2n	42.2	61.8	>128	>2.1
2o	44.4	>64	43.9	>0.7
2p	>64	>64	>128	ND
Isoniazid	0.1	0.3	ND	ND
Tamoxifen	ND	ND	11.1	ND

ND, not done.
[a] Fifty percent inhibitory concentration.
[b] Minimum inhibitory concentration.
[c] Fifty percent cytotoxicity concentration.
[d] Selectivity index (CC_{50}/MIC).

percentages. As depicted in Fig. 5, sixteen of the thiazolidinedione-hydroxamates were found antimycobacterial at a final test concentration of 100 μM. Only **2f**, **2h**, **2m** and **2o** completely lacked intracellular activity. Considering a final concentration of 10 μM, eight of the thiazolidinedione-hydroxamates showed an antimycobacterial activity in this experimental arrangement, namely **1b**, **1d**, **2a**, **2c**, **2e**, **2g**, **2i**, and **2k**. The percentage inhibition was 30.2, 21.6, 38.3, 46.9, 48.8, 19.4, 20.6 and 25.1%, respectively. This indicates that the existing structural differences not only influence the enzymatic inhibitory strength towards Zmp1 but also affect less straightforward biological properties such as cell membrane penetration. The hybrid **2n**, which showed only a low antimycobacterial activity against extracellular *Mtb* H37Ra, exhibited intracellular activity at the relatively high 100-μM concentration. In

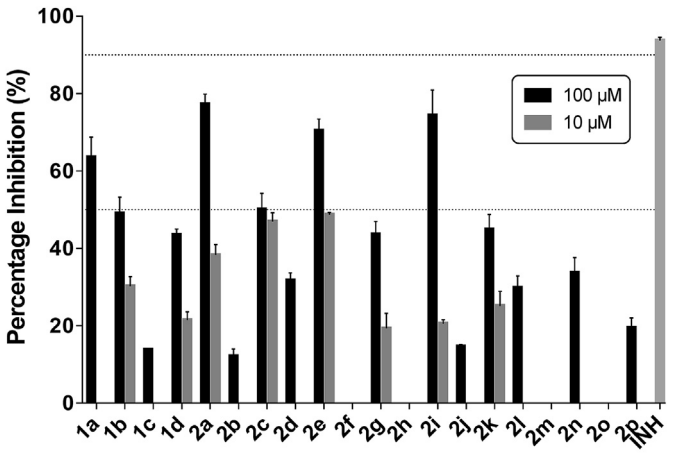

Fig. 5. Intracellular antimycobacterial activity of the thiazolidinedione-hydroxamates. The growth inhibition of Mtb H37Ra[lux] inside RAW264.7 macrophages upon 24 h of exposure to 100 and 10 μM of the hybrids was expressed as the percentage inhibition. Isoniazid (INH) was used as a reference at a final test concentration of 0.1 μM. Results are presented as the mean ± SD.

contrast, **2e** excels in antimycobacterial activity against intracellular residing *Mtb* H37Ra, even at the lower concentration of 10 μM, whereas it lacks a significant extracellular activity. Structure-activity relationship deductions indicate that the R^2 linker, connecting the thiazolidinedione and hydroxamate moieties, did not influence *in vitro* intracellular activity too much. In contrast, the R^1 substitution appeared largely influential. For example, for the simple thiazolidinedione-unsubstituted hydroxamates **1**, the benzyl-substitution (**1a** and **1c**) reduced intracellular antimycobacterial activity at lower concentrations. In contrast, the R^1 benzyl-substitution of the thiazolidinedione-hydroxamates **2** increased their *in vitro* potency against intracellular residing *Mtb* H37Ra. For the latter group, the R^3 substitution also showed to be important: the presence of an alkyl reduced the antimycobacterial activity at low concentrations, whereas substitution with either an unsubstituted benzyl group or fluorinated benzyl group increased the inhibition percentage in the intracellular test. Hybrid **2e** was selected as the most potent inhibitor of intracellular residing *Mtb* H37Ra, with an inhibition percentage of 70.4 and 48.8% at 100 and 10 μM, respectively. Hybrid **2n**, however, was selected as the most optimal compound considering the overall results, including the *in silico* drug-likeness predictions and target-based enzymatic assays.

3.4. Pose identification with in silico molecular docking

In order to explain the inhibitory effect of the thiazolidinedione-hydroxamates, we have employed a molecular docking of **2n** into the internal central cavity of *Mycobacterium tuberculosis* zinc metalloprotease Zmp1 structure (PDB ID: 3ZUK) [7]. The compound mimics the interactions of the indole part of phosphoramidon inhibitor crystal pose as shown in Fig. 6A. Both aromatic moieties, the indole of phosphoramidon and thiazolidinedione of compound **2n**, interact via a π-π interaction with the phenyl ring of F48. They also share the H-bond with R628 and the hydrophobic interactions with the aliphatic chain in the cleft formed by F48 and W604. Phosphoramidon, however, shows a direct interaction with the zinc atom and its surroundings leading towards much stronger inhibition ($K_i = 35$ nM according to PDBBIND) [42]. Compound **2n** shows additional polar contacts with the cavity entrance at R616. This is in agreement with the previous suggestion of designing such promising inhibitors, which would target the secondary binding pocket at the active site of Zmp1 [7].

The reasons for a good performance of the compound **2n** seem to be i) nonpolar aliphatic chain interaction with the hydrophobic cleft, where larger moieties do not fit, ii) unbranched linker joining the polar moiety of **2n** to the thiazolidinedione ring, which allows more flexibility towards the polar part of the entrance into the cavity and iii) polar interactions with highly populated charged residues within the entrance.

The studied thiazolidinedione-hydroxamates are thus expected to occupy the entrance into the central cavity, approximately 7 Å apart of the zinc-binding catalytic site (Fig. 6B). This is probably the reason for their lower efficiency than it could have been expected from their rational design (combining structural features of previously described potent inhibitors) as they are only gate-keeping the entry/exit of the peptidic substrate and do not further interfere with the reaction on the zinc atom. In contrast, as shown in crystal structures, phosphoramidon interacts directly with the zinc catalytic site and this allows the compound to inhibit also human zinc metallopeptidase neprilysin (NEP) structure (PDB ID: 1DMT) [43] as shown in Fig. 6C. NEP is able to cleave peptide bonds between hydrophobic residues in a variety of peptides such as opioid Met- and Leu-enkephalins [44] or angiotensins (e.g. angiotensin II). However, while the cleft surrounding the zinc-binding catalytic site is structurally identical, the entrance into the cavity differs

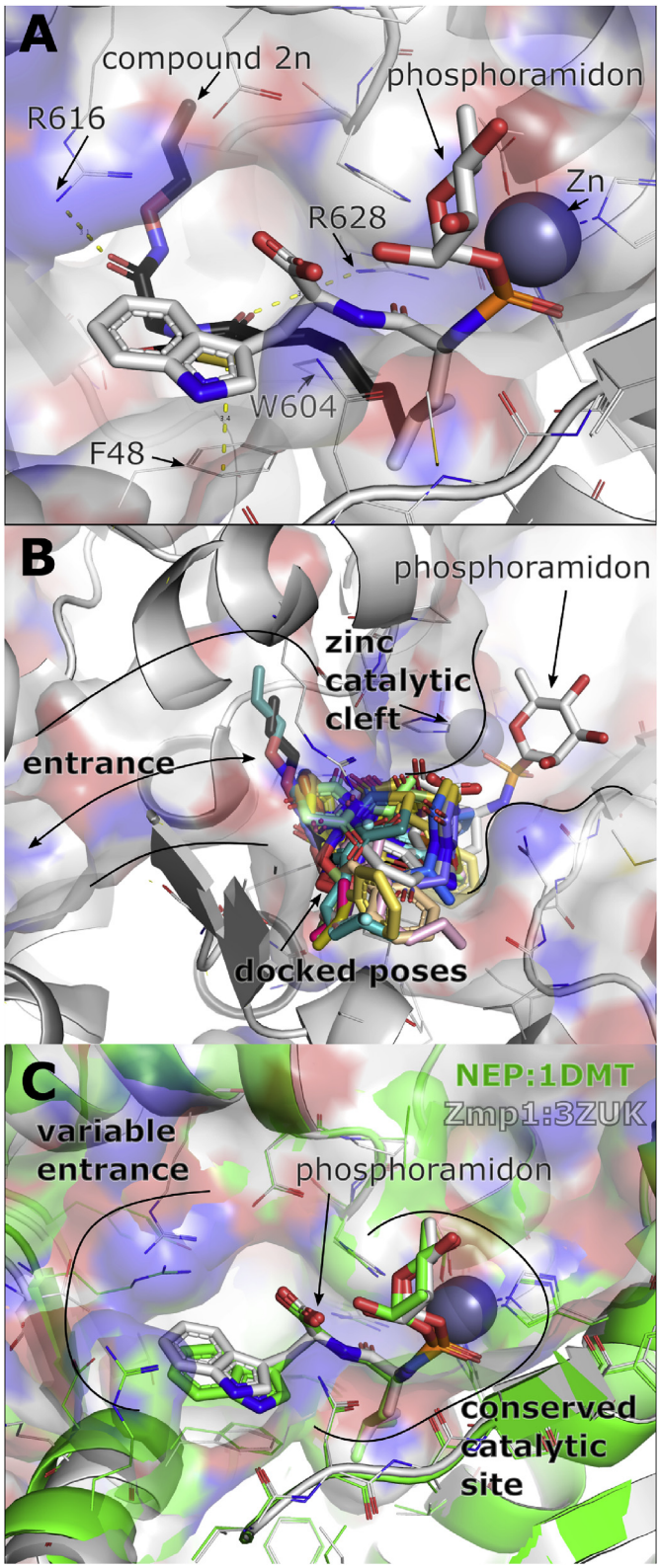

Fig. 6. Pose identification with molecular docking. A – a comparison of the docked pose of **2n** with that of phosphoramidon (from the crystal structure, PDB ID: 3ZUK) at the catalytic site of Zmp1; B – the docked poses of thiazolidinedione-hydroxamates in the entrance compared to the crystal structure pose of phosphoramidon blocking the entrance and also occupying the catalytic site of Zmp1; C – a comparison of the binding of phosphoramidon in the cavity of Zmp1 (PDB ID: 3ZUK) and neprilysin (NEP; PDB ID: 1DMT) [43]. Notice the conserved amino acids around the zinc-binding catalytic site; on the contrary, the entrance shows a variability in the constituting amino acids.

dramatically between the *Mycobacterium* and human zinc metallopeptidases.

4. Conclusion

In conclusion, we have developed an efficient synthetic protocol for the preparation of a series of thiazolidinedione-hydroxamates and assessed their inhibitory properties towards a recombinant Zmp1 from *Mycobacterium tuberculosis* by MALDI-TOF MS. This characterization was completed by whole-cell biological activity and cytotoxicity tests. Results showed that none of the synthesized thiazolidinedione-hydroxamates possessed acute cytotoxic effects against RAW264.7 macrophages. The extracellular anti-mycobacterial activity was rather limited, whereas anti-mycobacterial activity against intracellular residing bacilli was present for the majority of the tested hybrid library. The existing structural differences were reflected in the variability of the *in silico* predicted parameters and biologically determined responses. When looking for a synergic behavior of the studied synthetic compounds in all performed experimental tests, the compound **2n**, which does not contain aromatic R^1 and R^3 substituents as well as a branched R^2 linker, was found the most optimal.

5. Experimental section

5.1. Materials and methods

Solvents and chemicals were purchased from Sigma-Aldrich (www.sigmaaldrich.com) and Fluorochem (www.fluorochem.co.uk). All reactions were carried out at ambient temperature (21 °C) unless stated otherwise. Analytical thin-layer chromatography (TLC) was performed using aluminum plates precoated with silica gel (silica gel 60 F254).

The LC-MS analyses were carried out on UHPLC-MS system consisting of UHPLC chromatograph Accela with photodiode array detector and triple quadrupole mass spectrometer TSQ Quantum Access (Thermo Scientific, CA, USA), using Nucleodur Gravity C18 column (dimensions 1.8 μm, 2.1 × 50 mm at 30 °C and a flow rate of 800 μl/min (Macherey-Nagel, Germany). The mobile phase was (A) 0.1% ammonium acetate in water, and (B) 0.1% ammonium acetate in acetonitrile, linearly programmed from 10% to 80% B over 2.5 min, kept for 1.5 min. The column was re-equilibrated with 10% of solution B for 1 min. The APCI source operated at a discharge current of 5 μA, vaporizer temperature of 400 °C and a capillary temperature of 200 °C.

NMR 1H/13C spectra were recorded on JEOL ECX-500SS (500 MHz) or JEOL ECA400II (400 MHz) spectrometer at magnetic field strengths of 11.75 T (with operating frequencies 500.16 MHz for 1H and 125.77 MHz for 13C) and 9.39 T (with operating frequencies 399.78 MHz for 1H and 100.53 MHz for 13C) at ambient temperature (~21 °C). Chemical shifts (δ) are reported in parts per million (ppm), and coupling constants (J) are reported in Hertz (Hz). NMR spectra were recorded at ambient temperature (21 °C) in DMSO-d_6 and referenced to the resonance signal of the solvent.

HRMS analysis was performed with LC-MS and an Orbitrap high-resolution mass spectrometer (Dionex, Ultimate 3000, Thermo Exactive plus, MA, USA) operating in positive full scan mode in the range of 80–1200 *m/z*. The settings for electrospray ionization were as follows: 150 °C oven temperature and 3.6 kV source voltage. The acquired data were internally calibrated with phthalate as a contaminant in methanol (*m/z* 297.15909). Samples were diluted to a final concentration of 0.1 mg/ml in a solution of water and acetonitrile (50:50, v/v). The samples were injected into the mass spectrometer following HPLC separation on a Kinetex C18 column (2.6 μm, 100 A, 50 × 3.0 mm) using an isocratic mobile

phase of 0.01M acetonitrile/ammonium acetate (80/20) at a flow rate of 0.3 ml min^{-1}.

SFC chiral analyses were performed using an Acquity UPC system (Waters) consisting of a binary solvent manager, sample manager, column manager, column heater, convergence manager, PDA detector 2998, QDA mass detector and chiral analytical columns CHIRALPAK IA3, IB3, IC3 and ID3 (4,6 × 100 mm, 3 μm particle size). The chromatographic runs were performed at a flow rate of 2.2 ml min^{-1}, column temperature of 38 °C and ABPR 2000 psi.

5.2. Chemistry

5.2.1. General procedure for Knoevenagel condensation

A mixture of thiazolidinedione **3**, aldehyde (1 eq), piperidine (0.8 eq) and EtOH (130 ml/17 mmol) was refluxed on (16–20 h) and worked up according to *method A* or *B*.

Method A: The reaction mixture was poured into H_2O (200 ml), acidified with AcOH (10 ml) and filtered affording compounds **6**.

Method B: The product was concentrated *in vacuum* and purified by column chromatography (mobile phase: hexane/EtOAc 6:2) affording compounds **6**.

5.2.2. General procedure for reaction with bromoester

Thiazolidinedione **3** or **6** was dissolved in dry DMF (10 ml/8 mmol). NaH (1 eq) was slowly added to the reaction mixture followed by stirring and stirred for 10 min. Bromoester (1 eq) was added dropwise. After stirring overnight (24 h), the reaction mixture was diluted with water (50 ml). The product was extracted with DCM (5 × 50 ml), organic layers were washed with 5% HCl, brine, dried over Na_2SO_4 and concentrated in vacuum.

5.2.3. Methyl 2-(2,4-dioxo-5-pentylidenethiazolidin-3-yl)acetate 7a

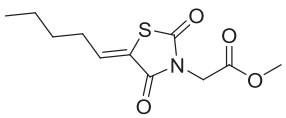

Orange oil. Yield: 81% (822 mg). ^{1}H NMR (500 MHz, DMSO-d_6): δ 7.12 (t, J = 7.7 Hz, 1H), 4.44 (s, 2H), 3.70 (s, 3H), 2.28–2.23 (m, 2H), 1.53–1.47 (m, 2H), 1.32 (dd, J = 14.9, 7.4 Hz, 2H), 0.89 (t, J = 7.3 Hz, 3H). ^{13}C NMR (126 MHz, DMSO-d_6): δ 167.17, 166.63, 163.57, 140.10, 123.92, 52.58, 41.83, 31.01, 29.23, 21.74, 13.56. HRMS: m/z: calcd for $C_{11}H_{15}NO_4S$: 258.0795 $[M+H]^+$; found: 258.0796.

5.2.4. Methyl 2-(2,4-dioxo-5-pentylidenethiazolidin-3-yl) propanoate 7b

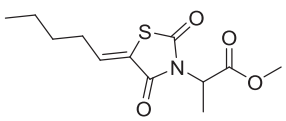

Mobile phase: DCM/MeOH 98:2. Brown solid. Yield: 44% (467 mg). ^{1}H NMR (500 MHz, DMSO-d_6): δ 7.10 (t, J = 7.7 Hz, 1H), 5.07 (q, J = 7.1 Hz, 1H), 3.65 (s, 3H), 2.24 (dd, J = 14.8, 7.5 Hz, 2H), 1.51–1.46 (m, 5H), 1.32 (dd, J = 14.9, 7.4 Hz, 2H), 0.89 (t, J = 7.3 Hz, 3H). ^{13}C NMR (126 MHz, DMSO-d_6): δ 169.02, 166.42, 163.42, 140.12, 123.77, 52.57, 49.98, 30.99, 29.24, 21.76, 13.95, 13.57. HRMS: m/z: calcd for $C_{12}H_{17}NO_4S$: 272.0951 $[M+H]^+$; found: 272.0952.

5.2.5. Ester hydrolysis

Ester **4/7** was dissolved in HBr 40% (8 ml/5 mmol) and refluxed for 5 h. The mixture was cooled down to rt and diluted with water (50 ml) and worked up according to *method A* or *B*.

Method A: The resulting suspension was filtered and washed with water.

Method B: The product was extracted with EtOAc (3 × 50 ml), washed with brine, dried over Na_2SO_4 and concentrated in vacuum.

5.2.6. 2-(2,4-Dioxo-5-(4-trifluoromethyl)benzylidene)thiazolidin-3-yl)propanoic acid 8a

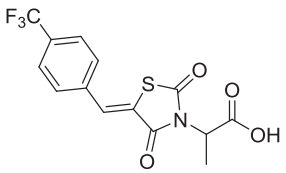

Method A. Brown solid. Yield: 55% (734 mg). ^{1}H NMR (500 MHz, DMSO-d_6): δ 13.28 (s, 1H), 8.06 (s, 1H), 7.91 (d, J = 8.4 Hz, 2H), 7.86 (d, J = 8.1 Hz, 2H), 5.03 (q, J = 7.2 Hz, 1H), 1.52 (d, J = 7.2 Hz, 3H). ^{13}C NMR (126 MHz, DMSO-d_6): δ 169.89, 166.32, 164.63, 136.83, 131.89, 130.63, 130.01 (q, J = 32.7 Hz), 126.12, 123.79 (q, J = 272.1 Hz), 123.68, 50.49, 13.87. HRMS: m/z: calcd for $C_{14}H_{10}F_3NO_4S$: 346.0355 $[M+H]^+$; found: 346.0358.

5.2.7. 2-(2,4-Dioxo-5-pentylidenethiazolidin-3-yl)propanoic acid 8b

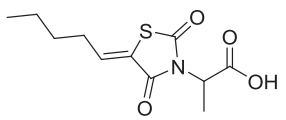

Method B. Brown solid. Yield: 83% (415 mg). ^{1}H NMR (500 MHz, DMSO-d_6): δ 13.16 (s, 1H), 7.08 (t, J = 7.7 Hz, 1H), 4.93 (q, J = 7.2 Hz, 1H), 2.24 (dd, J = 14.8, 7.5 Hz, 2H), 1.51–1.45 (m, 5H), 1.32 (dd, J = 14.9, 7.4 Hz, 2H), 0.89 (t, J = 7.3 Hz, 3H). ^{13}C NMR (126 MHz, DMSO-d_6): δ 169.97, 166.48, 163.58, 139.59, 123.94, 50.06, 30.96, 29.26, 21.76, 13.91, 13.57. HRMS: m/z: calcd for $C_{11}H_{15}NO_4S$: 258.0795 $[M+H]^+$; found: 258.0795.

5.2.8. Reaction with hydroxylamine.HCl

Carboxylic acid (1 eq) **5/8** was suspended in water (20 ml/1 mmol). Hydroxylamine.HCl (1.5 eq) was dissolved in water (20 ml/1 mmol). The amine mixture was added to the acid mixture and the pH was adjusted to 4.5 with 1M NaOH. THF was added until a homogeneous solution was obtained. EDC.HCl (3 eq) was dissolved in water (10 ml/1 mmol) and added in aliquots (4 ml/1 min) to the reaction mixture. The reaction was stirred for 2 h and worked up according to the *method A* or *B*.

Method A: The reaction was filtered and the solid was dried overnight.

Method B: The product was extracted with EtOAc (3 × 40 ml), washed with saturated $NaHCO_3$, brine, dried over Na_2SO_4 and concentrated *in vacuum.*

5.2.9. N-(benzyloxy)-2-(2,4-dioxothiazolidin-3-yl)acetamide 1a

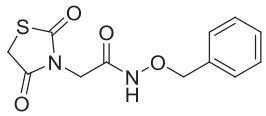

Method A. Mobile phase: DCM/MeOH 90:10. White solid. Yield: 49% (277 mg). ^{1}H NMR (500 MHz, DMSO-d_6): δ 11.22 (s, 1H), 7.42−7.35 (m, 5H), 4.82 (s, 2H), 4.25 (s, 2H), 4.10 (s, 2H). ^{13}C NMR (126 MHz, DMSO-d_6): δ 171.84, 171.46, 162.66, 135.65, 128.87, 128.32, 77.05, 41.14, 33.97. HRMS: *m*/*z*: calcd for $C_{12}H_{12}N_2O_4S$: 281.0591 $[M+H]^+$; found: 281.0592.

5.2.10. N-(allyloxy)-2-(2,4-dioxothiazolidin-3-yl)acetamide 1b

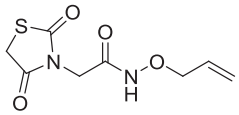

Method B. Mobile phase: $CHCl_3$/MeOH 90:10. Yellow oil. Yield: 55% (257 mg). ^{1}H NMR (500 MHz, DMSO-d_6): δ 11.35 (s, 1H), 5.95−5.87 (m, 1H), 5.31 (d, J = 17.3 Hz, 1H), 5.26 (d, J = 10.4 Hz, 1H), 4.27 (s, 4H), 4.03 (s, 2H). ^{13}C NMR (126 MHz, DMSO-d_6): δ 171.82, 171.44, 162.49, 132.70, 119.48, 76.05, 41.11, 33.96. HRMS: *m*/*z*: calcd for $C_8H_{10}N_2O_4S$: 231.0434 $[M+H]^+$; found: 231.0435.

5.2.11. N-(benzyloxy)-2-(2,4-dioxothiazolidin-3-yl)propanamide 1c

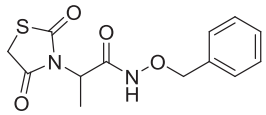

Method B. Mobile phase: DCM/MeOH 90:10. Yellow oil. Yield: 61% (342 mg). ^{1}H NMR (500 MHz, DMSO-d_6): δ 11.35 (s, 1H), 7.40−7.38 (m, 4H), 7.37−7.36 (m, 1H), 4.75 (d, J = 7.1 Hz, 2H), 4.68 (q, J = 7.1 Hz, 1H), 4.16 (s, 2H), 1.40 (d, J = 7.2 Hz, 3H). ^{13}C NMR (126 MHz, DMSO-d_6): δ 171.71, 171.31, 165.08, 135.67, 128.94, 128.28, 76.90, 49.39, 34.03, 13.61. HRMS: *m*/*z*: calcd for $C_{13}H_{14}N_2O_4S$: 295.0747 $[M+H]^+$; found: 295.0749.

5.2.12. N-(allyloxy)-2-(2,4-dioxothiazolidin-3-yl)propanamide 1d

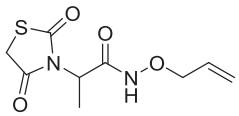

Method B. Mobile phase: $CHCl_3$/MeOH 90:10. Yellow oil. Yield: 52% (240 mg). ^{1}H NMR (500 MHz, DMSO-d_6): δ 11.24 (s, 1H), 5.94−5.86 (m, 1H), 5.30 (dd, J = 17.3, 1.6 Hz, 1H), 5.24 (d, J = 10.5 Hz, 1H), 4.65 (q, J = 7.1 Hz, 1H), 4.25−4.23 (m, 2H), 4.16 (s, 2H), 1.38 (d, J = 7.2 Hz, 3H). ^{13}C NMR (126 MHz, DMSO-d_6): δ 171.66, 171.29, 164.87, 132.80, 119.24, 75.83, 49.33, 34.02, 13.59. HRMS: *m*/*z*: calcd for $C_9H_{12}N_2O_4S$: 245.0591 $[M+H]^+$; found: 245.0593.

5.2.13. 2-(5-benzylidene-2,4-dioxothiazolidin-3-yl)-N-(benzyloxy) acetamide 2a

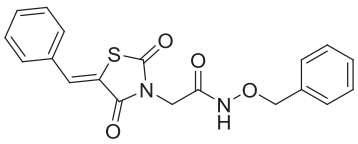

Method A. White solid. Yield: 58% (451 mg). ^{1}H NMR (500 MHz, DMSO-d_6): δ 11.34 (s, 1H), 7.96 (s, 1H), 7.65 (d, J = 7.3 Hz, 2H), 7.56 (t, J = 7.3 Hz, 2H), 7.52 (d, J = 7.1 Hz, 1H), 7.42−7.37 (m, 5H), 4.84 (s, 2H), 4.28 (s, 2H). ^{13}C NMR (126 MHz, DMSO-d_6): δ 166.96, 165.15, 162.54, 135.64, 133.50, 132.83, 130.77, 130.15, 129.39, 128.91, 128.33, 121.00, 77.10, 41.50. HRMS: *m*/*z*: calcd for $C_{19}H_{16}N_2O_4S$: 369.0904 $[M+H]^+$; found: 369.0907.

5.2.14. N-(allyloxy)-2-(5-benzylidene-2,4-dioxothiazolidin-3-yl) acetamide 2b

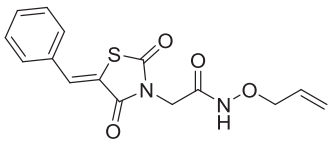

Method A. White solid. Yield: 51% (339 mg). ^{1}H NMR (500 MHz, DMSO-d_6): δ 11.26 (s, 1H), 7.96 (s, 1H), 7.64 (d, J = 6.0 Hz, 2H), 7.58−7.51 (m, 3H), 5.96 (s, 1H), 5.35 (d, J = 17.2 Hz, 1H), 5.28 (d, J = 9.2 Hz, 1H), 4.30 (d, J = 28.8 Hz, 4H). ^{13}C NMR (126 MHz, DMSO-d_6): δ 166.94, 165.13, 162.38, 133.48, 132.82, 132.69, 130.77, 130.14, 129.39, 120.99, 119.54, 76.09, 41.46. HRMS: *m*/*z*: calcd for $C_{15}H_{14}N_2O_4S$: 319.0747 $[M+H]^+$; found: 319.0749.

5.2.15. 2-(5-benzylidene-2,4-dioxothiazolidin-3-yl)-N-(benzyloxy) propanamide 2c

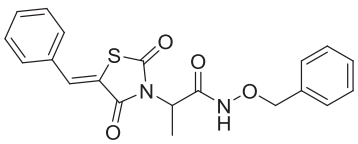

Method B. Mobile phase: DCM/MeOH 98:2. Yellow solid. Yield: 64% (373 mg). ^{1}H NMR (500 MHz, DMSO-d_6): δ 11.46 (s, 1H), 7.94 (s, 1H), 7.65 (d, J = 7.4 Hz, 2H), 7.58−7.50 (m, 3H), 7.40−7.34 (m, 5H), 4.87 (q, J = 7.1 Hz, 1H), 4.77 (q, J = 10.7 Hz, 2H), 1.50 (d, J = 7.2 Hz, 3H). ^{13}C NMR (126 MHz, DMSO-d_6): δ 166.75, 164.99, 164.90, 135.69, 132.96, 130.63, 130.05, 129.40, 128.97, 128.27, 121.36, 76.92, 49.85, 13.86. HRMS: *m*/*z*: calcd for $C_{20}H_{18}N_2O_4S$: 383.1060 $[M+H]^+$; found: 383.1058.

5.2.16. N-(allyloxy)-2-(5-benzylidene-2,4-dioxothiazolidin-3-yl) propanamide 2d

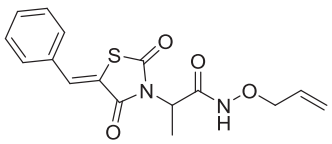

Method B. Mobile phase: DCM/MeOH 98:2. Yellow solid. Yield: 62% (314 mg). ^{1}H NMR (500 MHz, DMSO-d_6): δ 11.36 (s, 1H), 7.94 (s, 1H), 7.64 (d, J = 7.4 Hz, 2H), 7.58−7.51 (m, 3H), 5.91 (dq, J = 10.7,

6.1 Hz, 1H), 5.31 (d, $J = 17.3$ Hz, 1H), 5.24 (d, $J = 11.7$ Hz, 1H), 4.85 (q, $J = 7.1$ Hz, 1H), 4.26 (t, $J = 5.2$ Hz, 2H), 1.48 (d, $J = 7.2$ Hz, 3H). ^{13}C NMR (126 MHz, DMSO-d_6): δ 166.72, 164.98, 164.70, 132.95, 132.82, 130.63, 130.05, 129.39, 121.36, 119.30, 75.87, 49.81, 13.85. HRMS: *m/z*: calcd for $C_{16}H_{16}N_2O_4S$: 333.0904 $[M+H]^+$; found: 333.0905.

5.2.17. N-(benzyloxy)-2-(2,4-dioxo-5-(4-trifluoromethyl) benzylidene)thiazolidin-3-yl)acetamide 2e

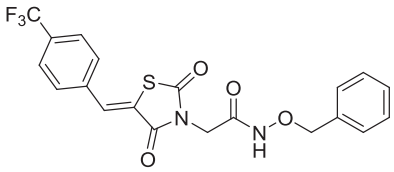

Method A. White solid. Yield: 49% (298 mg). ^{1}H NMR (500 MHz, DMSO-d_6): δ 11.35 (s, 1H), 8.04 (s, 1H), 7.87 (dd, $J = 19.3$, 8.2 Hz, 4H), 7.43–7.37 (m, 5H), 4.85 (s, 2H), 4.29 (s, 2H). ^{13}C NMR (126 MHz, DMSO-d_6): δ 166.62, 164.93, 162.45, 136.81, 135.63, 131.67, 129.97 (q, $J = 31.5$ Hz), 128.92, 128.33, 126.13, 124.00, 123.79 (q, $J = 273.4$ Hz), 77.11, 41.63. HRMS: *m/z*: calcd for $C_{20}H_{15}F_3N_2O_4S$: 437.0777 $[M+H]^+$; found: 437.0775.

5.2.18. N-(allyloxy)-2-(2,4-dioxo-5-(4-trifluoromethyl) benzylidene)thiazolidin-3-yl)acetamide 2f

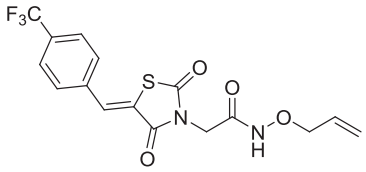

Method A. Yellow solid. Yield: 50% (289 mg). ^{1}H NMR (500 MHz, DMSO-d_6): δ 11.27 (s, 1H), 8.03 (s, 1H), 7.89 (d, $J = 8.4$ Hz, 2H), 7.85 (d, $J = 8.4$ Hz, 2H), 5.96 (dd, $J = 16.1$, 9.9 Hz, 1H), 5.35 (d, $J = 17.2$ Hz, 1H), 5.28 (d, $J = 10.1$ Hz, 1H), 4.33 (s, 4H). ^{13}C NMR (126 MHz, DMSO-d_6): δ 166.60, 164.91, 162.29, 136.81, 132.69, 131.66, 130.63, 129.97 (q, $J = 31.5$ Hz), 126.16, 124.00, 123.81 (q, $J = 272.1$ Hz), 119.56, 76.11, 41.59. HRMS: *m/z*: calcd for $C_{16}H_{13}F_3N_2O_4S$: 387.0621 $[M+H]^+$; found: 387.0621.

5.2.19. N-(benzyloxy)-2-(2,4-dioxo-5-(4-trifluoromethyl) benzylidene)thiazolidin-3-yl)propanamide 2g

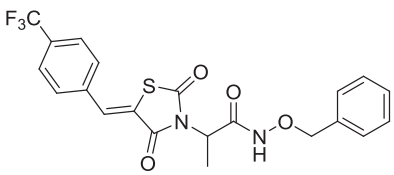

Method B. Mobile phase: DCM/MeOH 95:5. White solid. Yield: 48% (126 mg). ^{1}H NMR (500 MHz, DMSO-d_6): δ 11.47 (s, 1H), 8.03 (s, 1H), 7.91 (d, $J = 8.3$ Hz, 2H), 7.86 (d, $J = 8.1$ Hz, 2H), 7.41–7.34 (m, 5H), 4.88 (q, $J = 7.0$ Hz, 1H), 4.77 (q, $J = 8.4$ Hz, 2H), 1.50 (d, $J = 7.1$ Hz, 3H). ^{13}C NMR (126 MHz, DMSO-d_6): δ 166.41, 164.82, 164.78, 136.94, 135.67, 131.05, 130.53, 129.85 (q, $J = 32.7$), 128.98, 128.28, 126.16, 124.41, 123.80 (q, $J = 273.4$ Hz), 49.95, 13.82. HRMS: *m/z*: calcd for $C_{21}H_{17}F_3N_2O_4S$: 451.0934 $[M+H]^+$; found: 451.0934.

5.2.20. N-(allyloxy)-2-(2,4-dioxo-5-(4-trifluoromethyl) benzylidene)thiazolidin-3-yl)propanamide 2h

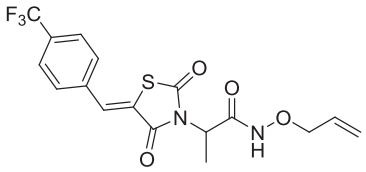

Method B. Mobile phase: DCM/MeOH 98:2. White solid. Yield: 31% (127 mg). ^{1}H NMR (500 MHz, DMSO-d_6): δ 11.37 (s, 1H), 8.02 (s, 1H), 7.91 (d, $J = 8.3$ Hz, 2H), 7.85 (d, $J = 8.2$ Hz, 2H), 5.91 (qd, $J = 11.8$, 6.1 Hz, 1H), 5.31 (d, $J = 17.3$ Hz, 1H), 5.24 (d, $J = 10.4$ Hz, 1H), 4.86 (q, $J = 6.9$ Hz, 1H), 4.26 (t, $J = 5.1$ Hz, 2H), 1.49 (d, $J = 7.1$ Hz, 3H). ^{13}C NMR (126 MHz, DMSO-d_6): δ 166.38, 164.76, 164.62, 136.94, 132.81, 131.04, 130.54, 129.85 (q, $J = 31.5$ Hz), 126.18, 124.41, 123.80 (q, $J = 272.1$ Hz), 119.34, 75.89, 49.92, 13.79. HRMS: *m/z*: calcd for $C_{17}H_{15}F_3N_2O_4S$: 401.0777 $[M+H]^+$; found: 401.0775.

5.2.21. N-(benzyloxy)-2-(5-(4-fluorobenzylidene)-2,4-dioxothiazolidin-3-yl)acetamide 2i

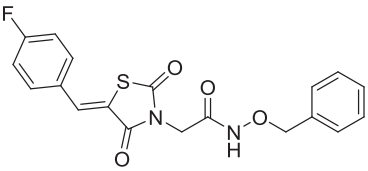

Method A. Yellow solid. Yield: 75% (617 mg). ^{1}H NMR (500 MHz, DMSO-d_6): δ 11.33 (s, 1H), 7.97 (d, $J = 7.0$ Hz, 1H), 7.71 (dd, $J = 12.5$, 6.7 Hz, 2H), 7.42–7.36 (m, 7H), 4.84 (s, 2H), 4.27 (s, 2H). ^{13}C NMR (126 MHz, DMSO-d_6): δ 166.85, 165.11, 164.06, 162.53, 162.06, 135.64, 132.66, 132.47, 129.51, 128.99, 128.82, 128,41, 128.26, 120.70, 116.74, 116.67, 116.43, 77.10, 41.51. HRMS: *m/z*: calcd for $C_{19}H_{15}FN_2O_4S$: 387.0809 $[M+H]^+$; found: 387.0813.

5.2.22. N-(allyloxy)-2-(5-(4-fluorobenzylidene)-2,4-dioxothiazolidin-3-yl)acetamide 2j

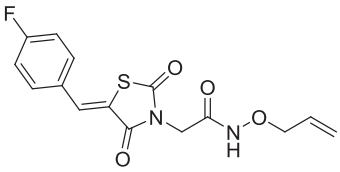

Method A. Yellow solid. Yield: 75% (432 mg). ^{1}H NMR (500 MHz, DMSO-d_6): δ 11.25 (s, 1H), 7.97 (s, 1H), 7.74–7.69 (m, 2H), 7.38 (t, $J = 8.4$ Hz, 2H), 5.95 (s, 1H), 5.35 (d, $J = 17.1$ Hz,2H), 5.28 (d, $J = 9.5$ Hz, 2H), 4.32 (br s, 4H). ^{13}C NMR (126 MHz, DMSO-d_6): δ 166.82, 165.10, 162.37, 162.06, 132.70, 132.62, 132.43, 129.50, 119.54, 116.72, 116.61, 116.55, 116.44, 76.09, 41.47. HRMS: *m/z*: calcd for $C_{15}H_{13}FN_2O_4S$: 337.0653 $[M+H]^+$; found: 337.0653.

5.2.23. N-(benzyloxy)-2-(5-(4-fluorobenzylidene)-2,4-dioxothiazolidin-3-yl)propanamide 2k

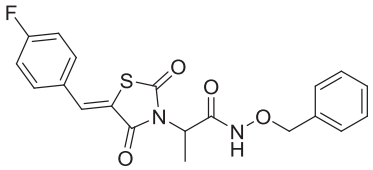

Method B. Mobile phase: DCM/MeOH 98:2. Green solid. Yield: 45% (62 mg). ^{1}H NMR (500 MHz, DMSO-d_6): δ 11.46 (s, 1H), 7.96 (s, 1H), 7.72 (dd, J = 8.5, 5.5 Hz, 2H), 7.43–7.34 (m, 7H), 4.87 (q, J = 7.1 Hz, 1H), 4.77 (d, J = 8.2 Hz, 2H), 1.49 (d, J = 7.2 Hz, 3H). ^{13}C NMR (126 MHz, DMSO-d_6): δ 166.63, 164.95, 164.89, 163.97, 161.97, 135.69, 132.59, 131.89, 129.62, 128.97, 128.27, 121.07, 116.68, 116.50, 76.92, 49.88, 13.86. HRMS: *m/z*: calcd for $C_{20}H_{17}FN_2O_4S$: 401.0966 $[M+H]^+$; found: 401.0968.

5.2.24. N-(allyloxy)-2-(5-(4-fluorobenzylidene)-2,4-dioxothiazolidin-3-yl)propanamide 2l

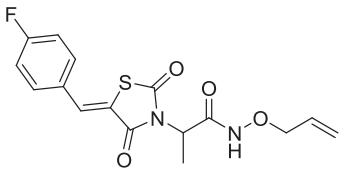

Method B. Mobile phase: DCM/MeOH 95:5. Green solid. Yield: 45% (54 mg). ^{1}H NMR (500 MHz, DMSO-d_6): δ 11.35 (s, 1H), 7.95 (s, 1H), 7.72 (dd, J = 8.7, 5.4 Hz, 2H), 7.41 (t, J = 8.8 Hz, 2H), 5.95–5.87 (m, 1H), 5.30 (d, J = 16.0 Hz, 1H), 5.24 (d, J = 10.4 Hz, 1H), 4.84 (q, J = 7.0 Hz, 1H), 4.26 (t, J = 5.2 Hz, 2H), 1.48 (d, J = 7.2 Hz, 3H). ^{13}C NMR (126 MHz, DMSO-d_6): δ 166.59, 164.94, 164.69, 161.97, 132.81, 132.59, 132.52, 131.88, 129.64, 121.07, 119.31, 116.67, 116.50, 75.88, 49.84, 13.84. HRMS: *m/z*: calcd for $C_{16}H_{15}FN_2O_4S$: 351.0809 $[M+H]^+$; found: 351.0811.

5.2.25. N-(benzyloxy)-2-(2,4-dioxo-5-pentylidenethiazolidin-3-yl) acetamide 2m

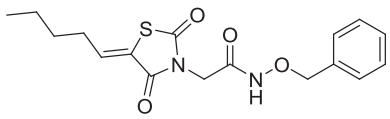

Method B. Brown solid. Yield: 35% (174 mg). ^{1}H NMR (500 MHz, DMSO-d_6): δ 11.29 (s, 1H), 7.43–7.37 (m, 5H), 7.09 (dt, J = 11.2, 7.6 Hz, 1H), 4.83 (d, J = 8.5 Hz, 2H), 4.21 (s, 2H), 2.27 (dq, J = 11.2, 7.4 Hz, 2H), 1.53 (dd, J = 14.5, 10.9 Hz, 2H), 1.36 (ddd, J = 14.5, 11.1, 7.5 Hz, 2H), 0.92 (t, J = 11.3, 7.3 Hz, 3H). ^{13}C NMR (126 MHz, DMSO-d_6): δ 166.79, 163.86, 162.60, 139.33, 135.64, 128.86, 128.33, 124.32, 77.07, 41.19, 30.95, 29.28, 21.75, 13.57. HRMS: *m/z*: calcd for $C_{17}H_{20}N_2O_4S$: 349.1217 $[M+H]^+$; found: 349.1217.

5.2.26. N-(allyloxy)-2-(2,4-dioxo-5-pentylidenethiazolidin-3-yl) acetamide 2n

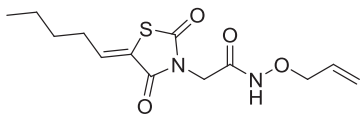

Method B. Mobile phase: hex/EtOAc 60:40. Yellow solid. Yield: 40% (178 mg). ^{1}H NMR (500 MHz, DMSO-d_6): δ 11.40 (s, 1H), 7.08 (t, J = 7.7 Hz, 1H), 5.91 (ddd, J = 16.5, 11.3, 6.0 Hz, 1H), 5.32 (d, J = 17.3 Hz, 1H), 5.26 (d, J = 10.4 Hz, 1H), 4.35–4.13 (m, 4H), 2.24 (dd, J = 14.7, 7.4 Hz, 2H), 1.50 (dt, J = 15.0, 7.4 Hz, 2H), 1.32 (dd, J = 14.9, 7.4 Hz, 2H), 0.89 (t, J = 7.3 Hz, 3H). ^{13}C NMR (126 MHz, DMSO-d_6): δ 166.76, 163.85, 162.43, 139.28, 132.70, 124.31, 119.48, 76.06, 41.16, 30.94, 29.27, 21.74, 13.57. HRMS: *m/z*: calcd for $C_{13}H_{18}N_2O_4S$: 299.1060 $[M+H]^+$; found: 299.1060.

5.2.27. N-(benzyloxy)-2-(2,4-dioxo-5-pentylidenethiazolidin-3-yl) propanamide 2o

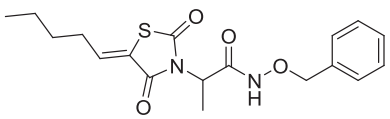

Method B. Mobile phase: DCM/MeOH 95:5. Yellow oil. Yield: 60% (160 mg). ^{1}H NMR (500 MHz, DMSO-d_6): δ 11.41 (s, 1H), 7.39–7.34 (m, 5H), 7.04 (t, J = 7.7 Hz, 1H), 4.76 (t, J = 8.8 Hz, 3H), 2.23 (q, J = 7.4 Hz, 2H), 1.51–1.48 (m, 2H), 1.45 (d, J = 7.2 Hz, 3H), 1.33 (dd, J = 14.9, 7.4 Hz, 2H), 0.89 (t, J = 7.3 Hz, 3H). ^{13}C NMR (126 MHz, DMSO-d_6): δ 166.59, 164.94, 163.73, 138.64, 135.68, 128.95, 128.26, 124.51, 76.89, 49.64, 30.87, 29.32, 21.75, 13.85, 13.59. HRMS: *m/z*: calcd for $C_{18}H_{22}N_2O_4S$: 363.1373 $[M+H]^+$; found: 363.1372.

5.2.28. N-(allyloxy)-2-(2,4-dioxo-5-pentylidenethiazolidin-3-yl) propanamide 2p

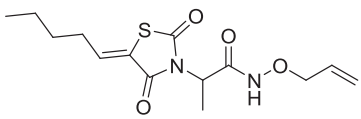

Method B. DCM/MeOH 85:15. Yellow oil. Yield: 56% (129 mg). ^{1}H NMR (500 MHz, DMSO-d_6): δ 11.31 (s, 1H), 7.04 (s, 1H), 5.91 (ddd, J = 17.0, 11.2, 5.9 Hz, 1H), 5.29 (d, J = 15.8 Hz, 1H), 5.23 (d, J = 8.8 Hz, 1H), 4.76 (q, J = 7.1 Hz, 1H), 4.24 (s, 2H), 2.23 (dd, J = 14.8, 7.4 Hz, 2H), 1.51–1.47 (m, 2H), 1.43 (d, J = 7.2 Hz, 3H), 1.33 (dd, J = 14.9, 7.4 Hz, 2H), 0.89 (t, J = 7.3 Hz, 3H). ^{13}C NMR (126 MHz, DMSO-d_6): δ 166.54, 164.74, 163.71, 138.63, 132.81, 119.25, 75.84, 49.59, 30.87, 29.32, 21.75, 13.84, 13.58. HRMS: *m/z*: calcd for $C_{14}H_{20}N_2O_4S$: 313.1217 $[M+H]^+$; found: 313.1215.

5.3. In silico prediction of drug-likeness properties

Physicochemical and pharmacokinetic parameters of the thiazolidinedione-hydroxamates were *in silico* predicted using the FAF*Drugs*4 [29] and admetSAR tools [30]. The different parameters predicted were as follows: molecular weight, octanol/water partition coefficient, number of hydrogen donors, number of hydrogen acceptors, number of atoms, number of rotatable bonds, aqueous solubility, Solubility Forecast Index, oral bioavailability via Veber's rule, 4/400 GSK rule, Ames toxicity and acute oral toxicity.

5.4. Zmp1 inhibition assay

Human angiotensin II (Sigma-Aldrich, Cat. No. A9525) was dissolved in LC-MS-quality water to a concentration of 4 nmol/ml. Aliquots (24 µl) of the stock solution were mixed with 1 µl of 2M NH_4HCO_3 in 0.5-ml test tubes. This was followed by pipetting either

Please cite this article as: V. Šlachtová et al., Novel thiazolidinedione-hydroxamates as inhibitors of *Mycobacterium tuberculosis* virulence factor Zmp1, European Journal of Medicinal Chemistry, https://doi.org/10.1016/j.ejmech.2019.111812

1 μl of neat acetone (control) or 1 μl of 1 mM inhibitor solution in acetone (sample). After pre-incubation in a thermostat at 37 °C for 3 min, the reaction was started by adding 1 μl of a recombinant Zmp1 metallopeptidase from *Mycobacterium tuberculosis* (ProSci, Poway, CA, USA; Cat. No. 90−361; diluted 1:4, *v/v*, with cold 50 mM NH_4HCO_3 and kept on ice during the measurements) and proceeded at 37 °C for 20 min. Aliquots (0.5 μl) of the reaction mixture were aspirated by a pipette each 2 min, spotted onto the MALDI target (an MSP BigAnchor 96 BC; Bruker Daltonik, Bremen, Germany), immediately overlaid with matrix solution (α-cyano-4-hydroxycinnamic acid, 5 mg/ml in acetonitrile: 2.5% (v/v) trifluoroacetic acid, 7:3, v/v), and left to dry and crystallize.

MALDI-TOF MS measurements were carried out on a Microflex LRF 20 instrument equipped with a 60-Hz nitrogen laser operating at $\lambda_{max} = 337$ nm (Bruker Daltonik). Mass spectra were accumulated from 1000 laser shots in the reflectron positive ion mode using an acceleration voltage (IS1) of 18.0 kV, extraction voltage (IS2) of 15.5 kV, lens voltage of 9.3 kV, reflectron voltage of 19.0 kV, detector voltage of 1590 V and pulsed ion extraction delay time of 350 ns The instrument was calibrated externally with a peptide mixture (Peptide Calibration Standard II; Bruker Daltonik).

The enzymatic reaction was monitored by the hydrolysis of angiotensin II yielding a peptide DRVY (*m/z* 552.3), which is accompanied by a simultaneous decrease in the angiotensin II signal (DRVYIHPF; *m/z* 1046.5). The ratio of *m/z* 552 versus *m/z* 1046 signal intensities was plotted against the reaction time to achieve an increasing linear dependence. The inhibition rate at the given inhibitor concentration of 40 μM was finally calculated by inverting the ratio of slopes for inhibited and control reaction. Phosphoramidone (RDF) was used as a reference inhibitor [16]. Three different inhibitor concentrations in the range of 20−80 μM were used to determine the corresponding IC_{50} value. The measured responses (percentages of inhibition) were plotted against the respective concentrations. All data points obtained for a single inhibitor were fitted by a straight line (linear regression equation: $y = a^*x + b$) and then IC_{50} (in μM) was obtained as a result of calculating formula (50 - b)/a.

5.5. In vitro antimycobacterial activity

In vitro activity of the synthesized hybrids against *Mtb* H37Ra (ATCC® 25177™) was evaluated by a resazurin assay. The thiazolidinedione-hydroxamates were solubilized in DMSO (Sigma-Aldrich) at stock concentration of 10 mM. A two-fold serial dilution of each compound was made in liquid Middlebrook 7H9 broth (Sigma-Aldrich) with 10% oleic acid, albumin, dextrose, catalase (OADC) enrichment (BD Biosciences; complete 7H9 broth) with final concentrations ranging from 64 to 0.25 μM. Volumes of 100 μl of the serial dilutions were added in triplicate to flat-bottomed 96-well plates. A mycobacterial suspension was prepared by thawing and dissolving a frozen glycerol-stock of *Mtb* H37Ra and, subsequently, diluting it in complete 7H9 broth to obtain a suspension with an appropriate inoculum size. A volume of 100 μl of the mycobacterial suspension was added to each well of the test plates. Isoniazid was used as a reference drug. Positive (100% growth) and negative (0% growth) controls were included as well. Test plates were incubated at 37 °C for 7 days. After 7 days of exposure, extracellular mycobacterial replication was assessed by resazurin. To each test well, 20 μl of a 0.02% resazurin (Sigma-Aldrich) solution was added. Test plates were incubated at 37 °C until a color change from blue to pink occurred. Fluorescence was measured at $\lambda_{ex} = 550$ nm and $\lambda_{em} = 590$ nm using a spectrophotometer (Promega Discover). Results were presented as the mean of triplicate values.

5.6. Assessment of acute in vitro cytotoxicity

The 50% cytotoxic concentration towards the RAW264.7 murine macrophage cell line (ATCC® TIB-71™) was determined by a neutral red uptake (NRU) assay. The RAW264.7 cells were cultured in Dulbecco's modified Eagle's medium (DMEM; Thermo Fisher) supplemented with 10% (v/v) heat-inactivated fetal calf serum (iFCS; Thermo Fisher) in a 5% CO_2 atmosphere at 37 °C until a semi-confluent layer of cells was obtained. Next, the cells were harvested and seeded into transparent, flat-bottomed 96-well plates at a density of 40.000 cells per well and left for recovery at 37 °C and 5% CO_2. The following day, twofold serial dilutions of the tested compounds were made in DMEM +10% iFCS with a final starting concentration of 128 μM. As a positive control, tamoxifen (Sigma-Aldrich) was included. The RAW264.7 cells were washed with sterile phosphate-buffered saline (PBS; Thermo Fisher) and exposed to the compounds by adding volumes of 100 μl of the serial dilutions. Tamoxifen was used as a reference drug. Test plates were left for 24 h at 37 °C and 5% CO_2. After 24 h exposure to the compounds, the cells were washed two times with sterile PBS and 100 μl neutral red (Sigma-Aldrich) working solution was added per well. Subsequently, the test plates were incubated for 3 h at 37 °C and 5% CO_2. The cells were washed again with sterile PBS and 150 μl of a 1:1 ethanol/acetic acid (Merck) mixture was added in each well. The plates were left shaking until the color became homogenous purple, and the optical density was measured at 530 nm and 620 nm (reference wavelength) using a plate reader (Promega Discover). Results were presented as the mean of triplicate values.

5.7. Macrophage infection assay

The intracellular activity of the thiazolidinedione-hydroxamates was tested by infecting the murine RAW264.7 macrophage cell line with *Mtb* H37Ra^{lux}, a laboratory *Mtb* H37Ra strain transformed with a pSMT1 luciferase reporter plasmid. The RAW264.7 cells were cultured, harvested and seeded into transparent, flat-bottomed 96-well plates as described above. Upon recovery, the cells were washed with sterile PBS and infected with H37Ra^{lux} at a multiplicity of infection (MOI) of 10 for 2 h at 37 °C. RAW264.7 cells were washed two times with sterile PBS, incubated with 100 μg/ml gentamicin (Sigma-Aldrich) for 1 h to kill the residual extracellular bacteria and, again, washed with sterile PBS. Then, the infected RAW264.7 cells were treated with the thiazolidinedione-hydroxamates at a final test concentration of 10 and 100 μM. Isoniazid was included as a reference drug at 0.1 μM. Uninfected cells were used as control. At 24 h post-exposure, the infected RAW264.7 cells were washed and lysed with 200 μl of 1% Triton X-100 (Sigma-Aldrich). To assess the intracellular mycobacterial replication, 25 μl of 1% (v/v) n-decanal in ethanol was added to 100 μl of the lysate and luminescence was measured using a luminometer (Promega Discover). Results were presented the mean of triplicate values.

5.8. In silico molecular docking

All 3D structures of the designed library of ligands were obtained with Marvin 15.1.5, software which can be used for drawing, displaying and characterization of chemical structure, substructures and reactions. Polar hydrogens were added to all ligands and proteins with the AutoDock Tools program [45]. Docking of the library of the structures into *Mycobacterium tuberculosis* zinc metalloprotease Zmp1 (PDB ID: 3ZUK) was carried out using AutoDock Vina 1.1.2 [46]. A grid box with the edge of 21 Å was centred on the active site of Zmp1 in the crystal structure (grid x: 95.8, y: 93.2, z: 33.0). The exhaustiveness parameter was set to 80 (default: 8).

Please cite this article as: V. Šlachtová et al., Novel thiazolidinedione-hydroxamates as inhibitors of *Mycobacterium tuberculosis* virulence factor Zmp1, European Journal of Medicinal Chemistry, https://doi.org/10.1016/j.ejmech.2019.111812

After docking, we compared the docked poses in bulk and that of the compound **2n** was further analyzed and interpreted.

Acknowledgements

This work was supported by grant no. JG_2019_002 from Palacký University in Olomouc.

Appendix A. Supplementary data

Supplementary data to this article can be found online at https://doi.org/10.1016/j.ejmech.2019.111812.

References

[1] M. Pai, M.A. Behr, M. Divangahi, D. Menzies, M. Pai, D. Dowdy, K. Dheda, C.C. Boehme, A. Ginsberg, S. Swaminathan, M. Spigelman, H. Getahun, M. Raviglione, Tuberculosis, Nat. Rev. Dis. Prim. 2 (2016) 16076.
[2] World Health Organization (WHO), Global Tuberculosis Report 2018, 2018 (Geneva).
[3] World Health Organization (WHO), WHO Consolidated Guidelines on Drug-Resistant Tuberculosis Treatment, 2019 (Geneva).
[4] World Health Organization (WHO), Implementing the End TB Strategy: the Essentials, 2015 (Geneva).
[5] K.C. Chang, C.C. Leung, E. Nuermberger, G. Sotgiu, New drugs and regimens for tuberculosis, Respirology 23 (2018) 978–990.
[6] R. Mehra, I.A. Khan, A. Nargotra, Anti-tubercular drug discovery: in silico implications and challenges, Eur. J. Pharm. Sci. 104 (2017) 1–15.
[7] D.M. Ferraris, D. Sbardella, A. Petrera, S. Marini, B. Amstutz, M. Coletta, P. Sander, M. Rizzi, Crystal structure of Mycobacterium tuberculosis zinc-dependent metalloprotease-1 (Zmp1), a metalloprotease involved in pathogenicity, J. Biol. Chem. 286 (2011) 32475–32482.
[8] S.S. Master, S.K. Rampini, A.S. Davis, C. Keller, S. Ehlers, B. Springer, G.S. Timmins, P. Sander, V. Deretic, *Mycobacterium tuberculosis* prevents inflammasome activation, Cell Host Microbe 3 (2008) 224–232.
[9] V. Lazarevic, F. Martinon, Linking inflammasome activation and phagosome maturation, Cell Host Microbe 3 (2008) 199–200.
[10] D.M. Ferraris, R. Miggiano, F. Rossi, M. Rizzi, *Mycobacterium tuberculosis* molecular determinants of infection, survival strategies, and vulnerable targets, Pathogens 7 (2018).
[11] D.M. Ferraris, M. Rizzi, Zinc-dependent Metalloprotease-1 (Zmp1), John Wiley & Sons Ltd., 2013, pp. 1–7.
[12] G. Hu, G. Lin, M. Wang, L. Dick, R.M. Xu, C. Nathan, H. Li, Structure of the *Mycobacterium tuberculosis* proteasome and mechanism of inhibition by a peptidyl boronate, Mol. Microbiol. 59 (2006) 1417–1428.
[13] A.F. Kisselev, Z. Songyang, A.L. Goldberg, Why does threonine, and not serine, function as the active site nucleophile in proteasomes? J. Biol. Chem. 275 (2000) 14831–14837.
[14] M. Mori, F. Moraca, D. Deodato, D.M. Ferraris, P. Selchow, P. Sander, M. Rizzi, M. Botta, Discovery of the first potent and selective *Mycobacterium tuberculosis* Zmp1 inhibitor, Bioorg. Med. Chem. Lett 24 (2014) 2508–2511.
[15] M. Mori, D. Deodato, M. Kasula, D.M. Ferraris, A. Sanna, A. De Logu, M. Rizzi, M. Botta, Design, synthesis, SAR and biological investigation of 3-(carboxymethyl)rhodanine and aminothiazole inhibitors of *Mycobacterium tuberculosis* Zmp1, Bioorg. Med. Chem. Lett 28 (2018) 637–641.
[16] M. Paolino, M. Brindisi, A. Vallone, S. Butini, G. Campiani, C. Nannicini, G. Giuliani, M. Anzini, S. Lamponi, G. Giorgi, D. Sbardella, D.M. Ferraris, S. Marini, M. Coletta, I. Palucci, M. Minerva, G. Delogu, I. Pepponi, D. Goletti, A. Cappelli, S. Gemma, S. Brogi, Development of potent inhibitors of the *Mycobacterium tuberculosis* virulence factor Zmp1 and evaluation of their effect on mycobacterial survival inside macrophages, ChemMedChem 13 (2018) 422–430.
[17] D.D. Subhedar, M.H. Shaikh, B.B. Shingate, L. Nawale, D. Sarkar, V.M. Khedkar, K.F. Kalam, J.N. Sangshetti, Quinolidene-rhodanine conjugates: facile synthesis and biological evaluation, Eur. J. Med. Chem. 125 (2017) 385–399.
[18] D.D. Subhedar, M.H. Shaikh, L. Nawale, A. Yeware, D. Sarkar, F.A. Kalam Khan, J.N. Sangshetti, B.B. Shingate, Novel tetrazoloquinoline-rhodanine conjugates: highly efficient synthesis and biological evaluation, Bioorg. Med. Chem. Lett 26 (2016) 2278–2283.
[19] S. Ponnuchamy, S. Kanchithalaivan, R. Ranjith Kumar, M. Ashraf Ali, T. Soo Choon, Antimycobacterial evaluation of novel hybrid arylidene thiazolidine-2,4-diones, Bioorg. Med. Chem. Lett 24 (2014) 1089–1093.
[20] N.B. Patel, I.H. Khan, Synthesis of newer 5-benzylidene-2,4-thiazolidinediones as potential antimicrobials, Indian J. Res. Pharm. Biotechnol. 2 (9) (2014) 993–1001.
[21] F.M. Shaikh, N.B. Patel, D. Rajani, Synthesis of new thiazolidine-2,4-dione derivatives and their antimicrobial and antitubercular activity, Indian J. Res. Pharm. Biotechnol. 1 (2013) 496–503.
[22] J.A. Jacobsen, J.L. Major Jourden, M.T. Miller, S.M. Cohen, To bind zinc or not to bind zinc: an examination of innovative approaches to improved metalloproteinase inhibition, Biochim. Biophys. Acta Mol. Cell Res. 1803 (2010) 72–94.
[23] M.W. Majewski, S. Cho, P.A. Miller, S.G. Franzblau, M.J. Miller, Syntheses and evaluation of substituted aromatic hydroxamates and hydroxamic acids that target *Mycobacterium tuberculosis*, Bioorg. Med. Chem. Lett 25 (2015) 4933–4936.
[24] M. Flipo, T. Beghyn, J. Charton, V.A. Leroux, B.P. Deprez, R.F. Deprez-Poulain, A library of novel hydroxamic acids targeting the metallo-protease family: design, parallel synthesis and screening, Bioorg. Med. Chem. 15 (2007) 63–76.
[25] Y.M. Lin, M.J. Miller, Practical synthesis of hydroxamate-derived siderophore components by an indirect oxidation method and syntheses of a DIG-siderophore conjugate and a biotin-siderophore conjugate, J. Org. Chem. 64 (1999) 7451–7458.
[26] K. Kar, U. Krithika, Mithuna, P. Basu, S. Santhosh Kumar, A. Reji, B.R. Prashantha Kumar, Design, synthesis and glucose uptake activity of some novel glitazones, Bioorg. Chem. 56 (2014) 27–33.
[27] S. Mohanty, A.K. Roy, V.K.P. Kumar, S.G. Reddy, A.C. Karmakar, Acetic anhydride-promoted one-pot condensation of 2,4-thiazolidinedione with bisulfite adducts of aldehydes, Tetrahedron Lett. 55 (2014) 4585–4589.
[28] U.R. Pratap, D.V. Jawale, R.A. Waghmare, D.L. Lingampalle, R.A. Mane, Synthesis of 5-arylidene-2,4-thiazolidinediones by Knoevenagel condensation catalyzed by Baker's yeast, New J. Chem. 35 (2011) 49–51.
[29] D. Lagorce, O. Sperandio, J.B. Baell, M.A. Miteva, B.O. Villoutreix, FAF-Drugs3: a web server for compound property calculation and chemical library design, Nucleic Acids Res. 43 (2015) W200–W207.
[30] F. Cheng, W. Li, Y. Zhou, J. Shen, Z. Wu, G. Liu, P.W. Lee, Y. Tang, admetSAR: a comprehensive source and free tool for assessment of chemical ADMET properties, J. Chem. Inf. Model. 52 (2012) 3099–3105.
[31] S. Chander, P. Ashok, D. Cappoen, P. Cos, S. Murugesan, Design, synthesis and biological evaluation of novel quinoline-based carboxylic hydrazides as anti-tubercular agents, Chem. Biol. Drug Des. 88 (2016) 585–591.
[32] S. Chander, P. Ashok, D. Cappoen, P. Cos, S. Murugesan, Design, synthesis and biological evaluation of novel quinoline-based carboxylic hydrazides as anti-tubercular agents, Chem. Biol. Drug Des. 88 (2016) 585–591.
[33] W.L. Jorgensen, E.M. Duffy, Prediction of drug solubility from Monte Carlo simulations, Bioorg. Med. Chem. Lett 10 (2000) 1155–1158.
[34] D.F. Veber, S.R. Johnson, H.Y. Cheng, B.R. Smith, K.W. Ward, K.D. Kopple, Molecular properties that influence the oral bioavailability of drug candidates, J. Med. Chem. 45 (2002) 2615–2623.
[35] J.A. Carson, T. Ansai, S. Awano, W. Yu, T. Takehara, A.J. Turner, Characterization of PgPepO, a bacterial homologue of endothelin-converting enzyme-1, Clin. Sci. (Lond.) 103 (Suppl 48) (2002) 90S–93S.
[36] M. Bucknall, K.Y.C. Fung, M.W. Duncan, Practical quantitative biomedical applications of MALDI-TOF mass spectrometry, J. Am. Soc. Mass Spectrom. 13 (2002) 1015–1027.
[37] N.V. Gogichaeva, T. Williams, M.A. Alterman, MALDI TOF/TOF tandem mass spectrometry as a new tool for amino acid analysis, J. Am. Soc. Mass Spectrom. 18 (2007) 279–284.
[38] Y. Zheng, X. Jiang, F. Gao, J. Song, J. Sun, L. Wang, X. Sun, Z. Lu, H. Zhang, Identification of plant-derived natural products as potential inhibitors of the *Mycobacterium tuberculosis* proteasome, BMC Complement Altern. Med. 14 (2014) 400–401, 400/7.
[39] E. Torfs, J. Vajs, M. Bidart de Macedo, F. Cools, B. Vanhoutte, Y. Gorbanev, A. Bogaerts, L. Verschaeve, G. Caljon, L. Maes, P. Delputte, P. Cos, J. Kosmrlj, D. Cappoen, Synthesis and in vitro investigation of halogenated 1,3-bis(4-nitrophenyl)triazenide salts as antitubercular compounds, Chem. Biol. Drug Des. 91 (2018) 631–640.
[40] R.J. Smets, E. Torfs, F. Lemiere, P. Cos, D. Cappoen, K. Abbaspour Tehrani, Synthesis and antitubercular activity of 1- and 3-substituted benzo[g]isoquinoline-5,10-diones, Org. Biomol. Chem. 17 (2019) 2923–2939.
[41] D. Cappoen, P. Claes, J. Jacobs, R. Anthonissen, V. Mathys, L. Verschaeve, K. Huygen, N.D. Kimpe, 1,2,3,4,8,9,10,11-Octahydrobenzo[j]phenanthridine-7,12-diones as New Leads against *Mycobacterium tuberculosis*, J. Med. Chem. 57 (2014) 2895–2907.
[42] R. Wang, X. Fang, Y. Lu, C.Y. Yang, S. Wang, The PDBbind database: methodologies and updates, J. Med. Chem. 48 (2005) 4111–4119.
[43] C. Oefner, A. D'Arcy, M. Hennig, F.K. Winkler, G.E. Dale, Structure of human neutral endopeptidase (neprilysin) complexed with phosphoramidon, J. Mol. Biol. 296 (2000) 341–349.
[44] A. Wisner, E. Dufour, M. Messaoudi, A. Nejdi, A. Marcel, M.N. Ungeeheuer, C. Rougeot, Human Opiorphin, a natural antinociceptive modulator of opioid-dependent pathways, Proc. Natl. Acad. Sci. U.S.A. 103 (2006) 17979–17984.
[45] G.M. Morris, R. Huey, W. Lindstrom, M.F. Sanner, R.K. Belew, D.S. Goodsell, A.J. Olson, AutoDock, AutoDockTools, Automated docking with selective receptor flexibility, J. Comput. Chem. 30 (2009) 2785–2791.
[46] O. Trott, A.J. Olson, AutoDock Vina, Improving the speed and accuracy of docking with a new scoring function, efficient optimization, and multithreading, J. Comput. Chem. 31 (2010) 455–461.

Please cite this article as: V. Šlachtová et al., Novel thiazolidinedione-hydroxamates as inhibitors of *Mycobacterium tuberculosis* virulence factor Zmp1, European Journal of Medicinal Chemistry, https://doi.org/10.1016/j.ejmech.2019.111812